Membrane Water Treatment, *Vol. 8, No. 1 (2017) 35-50*
DOI: https://doi.org/10.12989/mwt.2017.8.1.035

Performance improvement of countercurrent-flow membrane gas absorption in a hollow fiber gas-liquid membrane contactor

Chii-Dong Ho*, Yun-Jen Sung, Wei-Ting Chen and Feng-Chi Tsai

Energy and Opto-Electronic Materials Research Center, Department of Chemical and Materials Engineering, Tamkang University, Tamsui, New Taipei, 251, Taiwan

(*Received August 7, 2014, Revised August 22, 2016, Accepted October 4, 2016*)

Abstract. The theoretical membrane gas absorption module treatments in a hollow fiber gas-liquid membrane contactor using Happel's free surface model were obtained under countercurrent-flow operations. The analytical solutions were obtained using the separated variable method with an orthogonal expansion technique extended in power series. The CO_2 concentration in the liquid absorbent, total absorption rate and absorption efficiency were calculated theoretically and experimentally with the liquid absorbent flow rate, gas feed flow rate and initial CO_2 concentration in the gas feed as parameters. The improvements in device performance under countercurrent-flow operations to increase the absorption efficiency in a carbon dioxide and nitrogen gas feed mixture using a pure water liquid absorbent were achieved and compared with those in the concurrent-flow operation. Both good qualitative and quantitative agreements were achieved between the experimental results and theoretical predictions for countercurrent flow in a hollow fiber gas-liquid membrane contactor with accuracy of $6.62\times10^{-2}\leq E\leq8.98\times10^{-2}$.

Keywords: countercurrent flow; membrane gas absorption; hollow fiber module; conjugated Graetz problem

1. Introduction

The membrane-based gas absorption process is established using a hydrophobic microporous membrane that permits the gas species to be separated by diffusing first through the membrane pores. The gas absorption then occurs at the hydrophobic membrane pore mouth on the liquid absorbent side (Li and Teo 1998, Karoor and Sirkar 1993). The membrane contactor application to the gas absorption process is aimed at avoiding problems, such as foaming, unloading, flooding, entraining and channeling which are often encountered in the traditional absorption module device. Membrane gas absorption processes have gained increasing attention in the past few years due to their operational flexibility, high mass transfer rate and scaling up ease (Mavroudi, Kaldis *et al.* 2003, Al-Marzouqi, El-Nass *et al.* 2008, Zhang, Wang *et al.* 2008) in enhancing absorption system separation efficiency.

The most common hollow fiber membrane contactor device was designed in a shell-tube configuration with both shell- and lumen-side fluids flowing in parallel (Lee, Noble *et al.* 2001,

*Corresponding author, Ph.D., E-mail: cdho@mail.tku.edu.tw

http://www.techno-press.org/?journal=mwt&subpage=7 ISSN: 2005-8624 (Print), 2092-7037 (Online)

Gabelman and Hwang 1999, Kim and Yang 2000). This device was applied to liquid/liquid and gas/liquid separation processes and widely used in fermentation (Bothuna, Knutsona *et al.* 2003), pharmaceuticals (Laouinia, Jaafar-Maaleja *et al.* 2011), wastewater treatment (Rezakazemi, Shirazian *et al.* 2012), metal ion extraction (Ramakula, Prapasawada *et al.* 2007), VOC removal from waste gas (Li, Xu *et al.* 2009) and osmotic distillation (Varavuth, Jiraratananon *et al.* 2009). A mathematical model was developed that combined the mass transfer resistances on the shell side (Yang and Cussler 1986, Costello, Fane *et al.* 1993) in liquid film and gas solute distribution coefficient between the gas and liquid phases to estimate the overall mass transfer coefficient (Qi and Cussler 1985a, 1985b, Dindore, Brilman *et al.* 2004).

A hydrophobic hollow-fiber membrane contactor was implemented in this study for CO_2 removal from a gas feed using water as the liquid absorbent. The liquid absorbent was assumed to flow through the shell side and CO_2/N_2 gas mixture with a volume ratio as the gas feed flowing into the fiber side. Microporous hydrophobic membranes are employed as the contactor interface for CO_2 transfer. The formulation for such a coupled boundary value problem using Happel's free surface model (Happel 1959) in countercurrent-flow hollow-fiber gas absorption operation, referred to as conjugated Graetz problems (Perelman 1961, Davis and Venkatesh 1979, Papoutsakis and Ramkrishna 1981), is developed theoretically and validated experimentally in this work. The analytical solution for such a conjugated Graetz problem was obtained using the orthogonal technique and separated variables method (Nunge and Gill 1966, Ho, Yeh *et al.* 1998). The availability of such a simplified mathematical formulation and the solution methodology to predict the absorption efficiency and two-dimensional concentration profiles as developed here for hollow-fiber membrane modules is the value of the present work. The total absorption rate and absorption efficiency of the shell-and-tube membrane contactor was investigated to find a better device performance for the hollow fiber membrane gas absorption process under various operating parameters, such as absorbent flow rate, gas feed flow rate and initial CO_2 concentration in the gas feed. The total absorption rate and absorption efficiency for both concurrent-flow and countercurrent-flow operations were also evaluated for comparison.

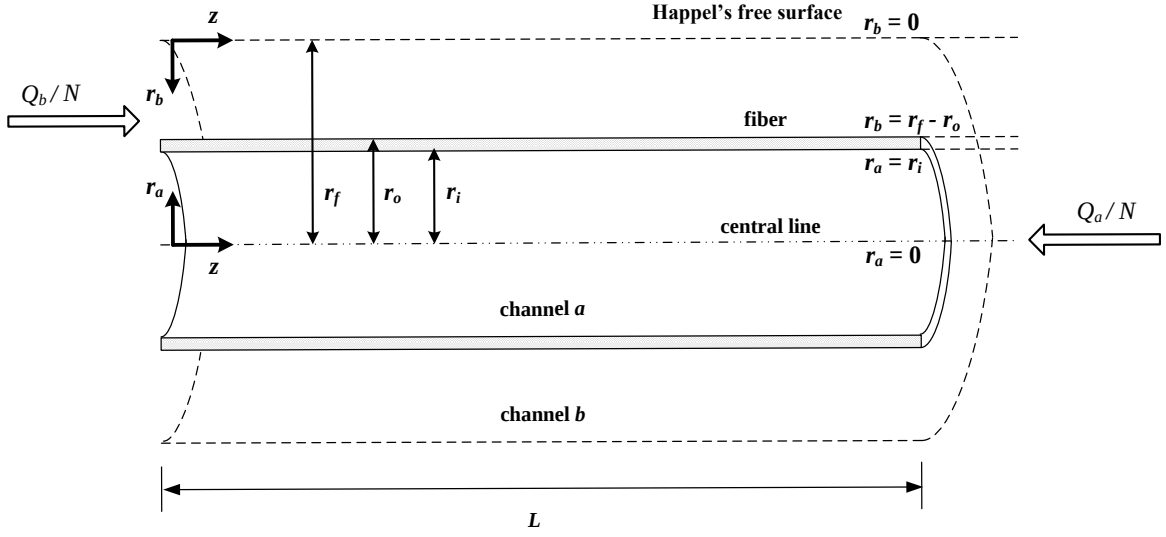

Fig. 1 Schematic diagram of Happel's free surface model in hollow fiber membrane module

2. Mathematical statements

Fig. 1 shows a hollow-fiber membrane module with gas feed flowing into membrane fiber cells and the liquid absorbent entering the shell side to conduct a countercurrent-flow gas absorption process. The outlet CO_2 concentrations in the liquid absorbent were measured to estimate the total amount of gas absorbed by the liquid absorbent. The mathematical formulation for the mass transfer phenomena for such modules was proposed by Happel (1959) with an imaginary outer boundary in the fiber cell, the so called "free surface". Considering only the mass transfer characteristics on the shell side was further investigated by Zhang, Wang *et al.* (2003) assuming a uniformly packed hollow-fiber module and ignoring the velocity profile across the module radius direction. Two radial coordinates, as shown in Fig. 1, were proposed to simplify the mathematical treatment in a simplified expression, and there is actually no need to neglect the hollow fiber membrane thickness, however, the fiber-curvature effect in the boundary condition Eq. (7) is neglected with respect to the hollow fiber radius, as shown in Fig. 1, the following assumptions are made: (1) steady-state fully-developed laminar flow in each fiber cell and only the longitudinal velocity component exists; (2) negligible axial diffusion; constant physical properties in isothermal operations; (3) Henry's law applicability; (4) Happel's surface model is used to characterize the velocity profile on the shell side; (5) the fiber cell membrane thickness is neglected compared to the hollow fiber radius. Based on these assumptions, the mathematical formulations for the shell-and-tube module in the hollow-fiber membrane contactor performed the same as in the previous works (Ho, Sung *et al.* 2013, Wang, Lin *et al.* 2006) except the velocity distributions and boundary conditions for the countercurrent-flow operations in the dimensionless forms are as follows

$$v_a(\eta_a) = -2\overline{v_a}\left[1-\left(\frac{\eta_a}{\eta_i}\right)^2\right] \quad \text{for the fiber side} \tag{1}$$

$$v_b(\eta_b) = \frac{2\overline{v_b}}{\left[\left(\frac{2}{\eta_m^2}-3\right)+\eta_o^2\right]}\left[\eta_o^2-(1-\eta_b)^2+2\ln\left(\frac{1-\eta_b}{\eta_o}\right)\right] \quad \text{for the shell side} \tag{2}$$

$$\psi_a(\eta_a,1) = \psi_{ai} \tag{3}$$

$$\psi_b(\eta_b,0) = \psi_{bi} \tag{4}$$

$$\frac{\partial\psi_a(0,\xi)}{\partial\eta_a} = 0 \tag{5}$$

$$\frac{\partial\psi_b(0,\xi)}{\partial\eta_b} = 0 \tag{6}$$

$$-\frac{\partial\psi_a(\eta_i,\xi)}{\partial\eta_a} = \frac{\varepsilon r_f}{\delta}\left[\psi_a(\eta_i,\xi)-\frac{1}{H}\psi_b(1-\eta_o,\xi)\right] \tag{7}$$

Table 1 The dimensionless outlet concentration in the both phase for the eigenvalue number and expansion coefficients with analytical solution for countercurrent-flow operations, Gz_a=0.062741, Gz_a=400

m	λ_0	Λ_1	Λ_2	Λ_3	$S_{a,0}$	$S_{b,0}$	$S_{a,1}$	$S_{b,1}$	$S_{a,2}$	$S_{b,2}$	$S_{a,3}$	$S_{b,3}$	$\overline{\psi}_{ae}$	$\overline{\psi}_{be}$
1	0.0	0.06	-	-	-0.1393	-0.1158	0.9368	0.1398	-	-	-	-	0.7975	0.0545
2	0.0	0.06	-0.265	-	-0.1484	-0.1234	0.9921	0.1481	-0.037	0.0656	-	-	0.8065	0.0520
3	0.0	0.06	-0.265	-0.848	-0.1454	-0.1209	0.9743	0.1454	-0.0355	0.063	0.0121	0.0376	0.8053	0.0523

$$-\frac{\partial \psi_a(\eta_i,\xi)}{\partial \eta_a}=\frac{\eta_o D_{AC}}{\eta_i D_{AB}}\frac{\partial \psi_b(1-\eta_o,\xi)}{\partial \eta_b} \tag{8}$$

in which

$$\overline{v}_a=\frac{Q_a}{\pi r_i^2},\ \overline{v}_b=\frac{Q_b}{\pi r_f^2-\pi r_o^2},\ r_f=\frac{r_o}{\sqrt{\phi}},\ \eta_a=\frac{r_a}{r_f},\ \eta_b=\frac{r_b}{r_f},\ \eta_i=\frac{r_i}{r_f},\ \eta_o=\frac{r_o}{r_f},$$

$$\eta_m=\sqrt{\frac{1-\eta_o^2}{2\ln\frac{1}{\eta_o}}},\ \xi=\frac{z}{L},\ \psi_a=\frac{C_a}{C_{ai}-C_{bi}},\ \psi_b=\frac{C_b}{C_{ai}-C_{bi}},\ Gz_a=\frac{\overline{v}_a r_f^2}{LD_{AB}},\ Gz_b=\frac{\overline{v}_b r_f^2}{LD_{AC}} \tag{9}$$

where ε is the membrane permeability and H is the dimensionless Henry's law constant (Versteeg and van Swaaij 1998). Four eigenvalues and the associated expansion coefficients were calculated using the physical properties and operating conditions. Some results for Gz_a=0.062741, Gz_b=400 as well as the dimensionless outlet concentration are shown in Table 1. It was found that the power-series expressions for the concentration distributions converge very rapidly and only three eigenvalues as well as their corresponding eigenfunctions are necessary consideration during the calculation procedure, as indicated from Table 1. The concentration distributions along the flow direction of both the shell and fiber sides are obtained in terms of the mass-transfer Graetz number (Gz_a and Gz_b), eigenvalues (λ_m), expansion coefficients ($S_{a,m}$ and $S_{b,m}$) and eigenfunctions ($F_{a,m}$ and $F_{b,m}$). The results are

$$\psi_a(\eta_a,\xi)=S_{a,0}+\sum_{m=1}^{\infty}S_{a,m}F_{a,m}(\eta_a)G_m(\xi) \tag{10}$$

$$\psi_b(\eta_b,\xi)=S_{b,0}+\sum_{m=1}^{\infty}S_{b,m}F_{b,m}(\eta_b)G_m(\xi) \tag{11}$$

We can define the dimensionless average concentration with the aid of Eqs. (10) and (11) for both the gas feed and liquid absorbent as follows

$$\overline{\psi_a}(\xi)=S_{a,0}-\frac{2}{Gz_a\eta_i}\sum_{m=1}^{\infty}\frac{1}{\lambda_m}S_{a,m}F_{a,m}'(\eta_i)e^{\lambda_m\xi} \tag{12}$$

$$\overline{\psi_b}(\xi)=S_{b,0}+\frac{2\eta_o}{Gz_b}\sum_{m=1}^{\infty}\frac{1}{\lambda_m}S_{b,m}F_{b,m}'(1-\eta_o)e^{\lambda_m\xi} \tag{13}$$

3. Total absorption rate and absorption efficiency

The local liquid absorbent Sherwood number is defined using

$$k_{b\xi}=\frac{D_{AC}}{r_f}\frac{\partial\psi_b(1-\eta_o,\xi)/\partial\eta_b}{\psi_b(1-\eta_o,\xi)-\overline{\psi_b}(\xi)} \tag{14}$$

where $k_{b\xi}$ is the local mass transfer coefficient for liquid absorbent and D_{eq}=2(r_f–r_o) is the equivalent diameter of the shell side. The numerator and denominator in Eq. (14) are obtained with the differentiation of Eq. (11) and the substitution of Eqs. (11) and (13) as follows

$$\partial\psi_b(1-\eta_o,\xi)/\partial\eta_b=\sum_{m=1}^{\infty}S_{b,m}F'_{b,m}(1-\eta_o)e^{\lambda_m\xi} \tag{15}$$

$$\psi_b(1-\eta_o,\xi)-\overline{\psi_b}(\xi)=\sum_{m=1}^{\infty}S_{b,m}\left[F_{b,m}(1-\eta_o)-\frac{2\eta_o}{Gz_b\lambda_m}F'_{b,m}(1-\eta_o)\right]e^{\lambda_m\xi} \tag{16}$$

The final local Sherwood number form in Eq. (14) was expressed in terms of the eigenfunctions and expansion coefficients using Eqs. (15) and (16) as

$$Sh_{\xi}=\frac{k_{b\xi}D_{eq}}{D_{AC}}=\frac{2(1-\eta_o)\sum_{m=1}^{\infty}S_{b,m}F'_{b,m}(1-\eta_o)e^{\lambda_m\xi}}{\sum_{m=1}^{\infty}S_{b,m}\left[F_{b,m}(1-\eta_o)-\frac{2\eta_o}{Gz_b\lambda_m}F'_{b,m}(1-\eta_o)\right]e^{\lambda_m\xi}} \tag{17}$$

Hence, the average Sherwood number can be obtained accordingly

$$\overline{Sh}=\int_0^1 Sh_{\xi}d\xi=\int_0^1\frac{2(1-\eta_o)\sum_{m=1}^{\infty}S_{b,m}F'_{b,m}(1-\eta_o)e^{\lambda_m\xi}}{\sum_{m=1}^{\infty}S_{b,m}\left[F_{b,m}(1-\eta_o)-\frac{2\eta_o}{Gz_b\lambda_m}F'_{b,m}(1-\eta_o)\right]e^{\lambda_m\xi}}d\xi \tag{18}$$

The total absorption rate and absorption efficiency were estimated using Eq. (19) with plugging in both the tube- and shell-side outlet concentrations into Eqs. (12) and (13), respectively

$$\omega=Q_b\left(\overline{C_{be}}-\overline{C_{bi}}\right)=2\pi LD_{AC}\eta_o(C_{ai}-C_{bi})\sum_{m=1}^{\infty}\frac{1}{\lambda_m}S_{b,m}F'_{b,m}(1-\eta_o)\left(e^{\lambda_m}-1\right) \tag{19}$$

and

$$I_M=\frac{\overline{\psi_{ai}}-\overline{\psi_{ae}}}{\overline{\psi_{ai}}}\times100\%=\frac{\sum_{m=1}^{\infty}\frac{1}{\lambda_m}S_{a,m}F'_{a,m}(\eta_i)\left(1-e^{\lambda_m}\right)}{\left[\frac{Gz_a\eta_i}{2}S_{a,o}+\sum_{m=1}^{\infty}\frac{1}{\lambda_m}S_{a,m}F'_{a,m}(\eta_i)\right]}\times100\% \tag{20}$$

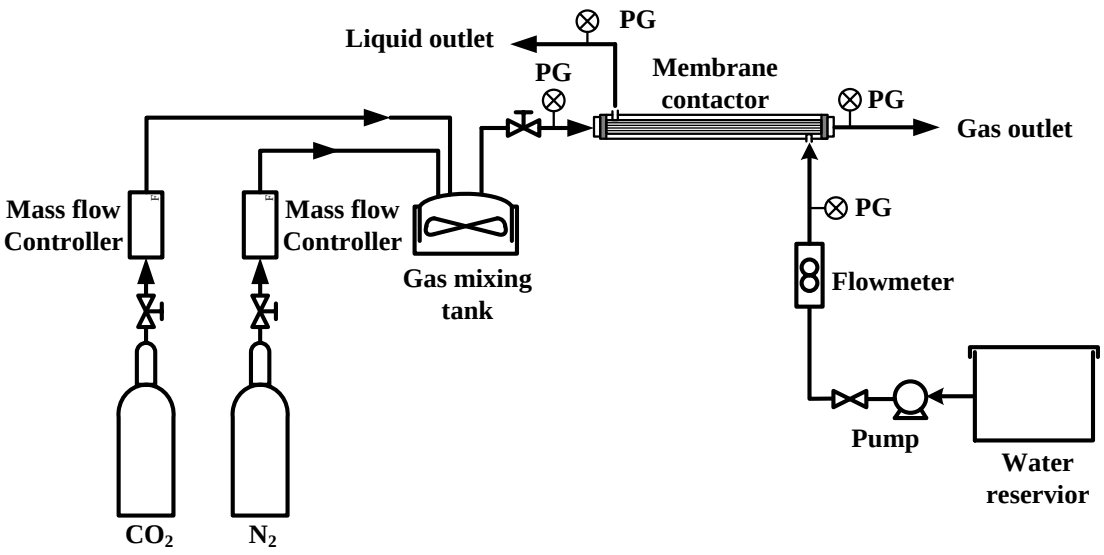

Fig. 2 Schematic diagram of the experimental setup

Table 2 Characteristics of hollow fiber membrane module and physical properties of carbon dioxide

hollow fiber membrane module	PVDF
Length of fibers (m)	0.31
Membrane surface area (m^2)	0.0321
Inner diameter of shell (mm)	15
Inner diameter of fiber cell (mm)	1.4
Outer diameter of fiber call (mm)	2.2
Membrane thickness (μm)	134
Average pore size (μm)	2
Membrane porosity	0.6
Total number of fibers	15
Packing density of the hollow fibers	0.323
Henry's law constant	H=0.8314
ordinary diffusion coefficient of CO_2 in N_2	$D_{AB}=1.67\times10^{-5}$ m^2/s
ordinary diffusion coefficient of CO_2 in water	$D_{ACc}=2\times10^{-9}$ m^2/s

4. Experimental apparatus

An experimental countercurrent-flow hollow fiber gas-liquid membrane contactor module is shown in Fig. 2. The hydrophobic PVDF hollow-fiber membrane module (Microza, PALL) characteristics and the carbon dioxide physical properties are presented in Table 2. The mathematical formulation is applicable to the present work with the packing density $\phi<0.4$ (Happel 1959). Less than 2 μs/cm conductance distilled water was used during all experimental runs. The experimental runs were carried out in a hollow-fiber module as a permeable barrier to absorb CO_2 from a CO_2/N_2 gas mixture using three initial CO_2 concentrations in a 10, 20 and 30%, gas mixture

feed at a gas feed flow rate of 2 and 3 cm^3/s and liquid absorbent flow rate between 0.25~3 cm^3/s. The absorption efficiency was determined using the amount of CO_2 in the gas feed absorbed into the water absorbent. The outlet water stream was analyzed using a total organic carbon analyzer (Model 1010 TOC analyzer, O.I. Corporation) at 10 minute intervals until the steady state condition was reached with no further change in CO_2 concentration in the water absorbent. A peristaltic pump (Masterflex, L/S No.77200-12) was used including the EASY-LOAD pump head (model 7518-00) and a rotameter (Fong-JEI) to control the liquid absorbent flow rate while a gas feed mass flow controller (Hastings, HFC-202C) was implemented to regulate the gas feed flow rate.

5. Results and discussions

The dimensionless outlet concentration, average Sherwood number, total absorption rate and

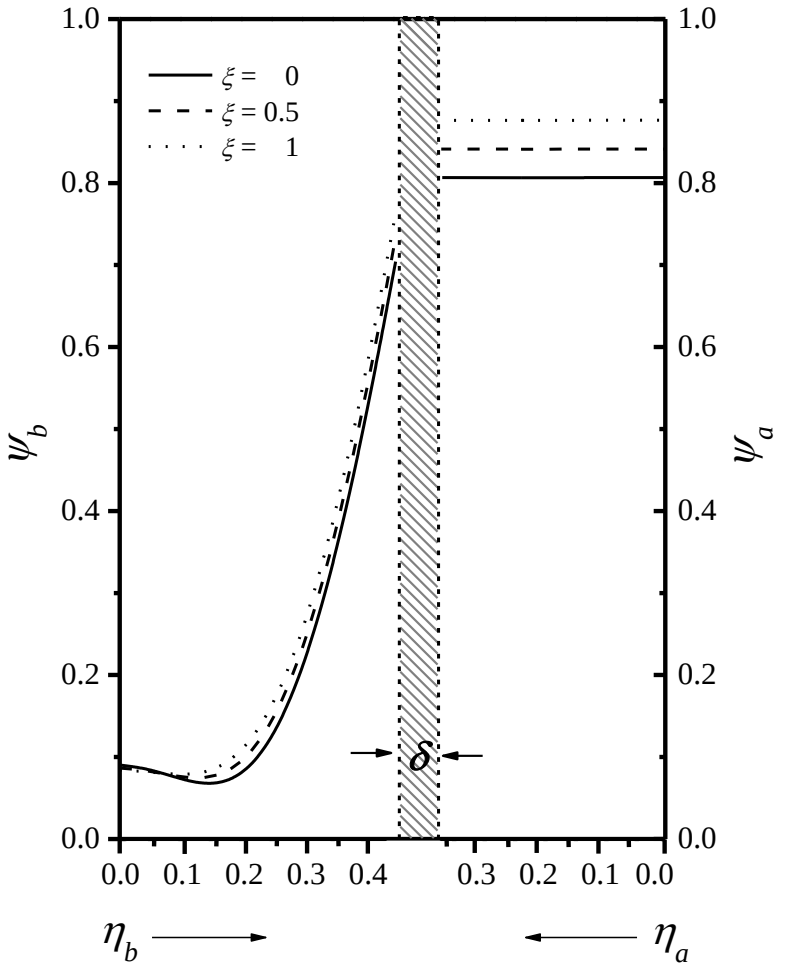

Fig. 3 Transverse concentration distributions in both gas feed and liquid absorbent (Gz_a=0.0627, Gz_b=400)

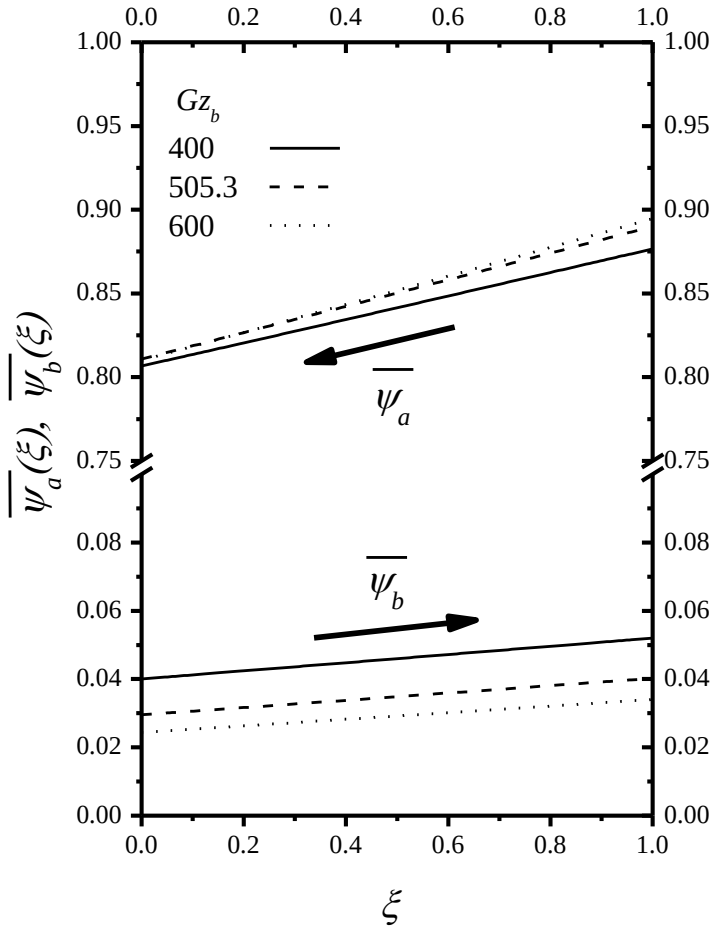

Fig. 4 Average concentration distribution in liquid absorbent within whole membrane contactor with mass-transfer Graetz number Gz_b as a parameter for Gz_a=0.0627

absorption efficiency were calculated from Eqs. (12), (13), (18), (19) and (20), respectively.

5.1 The dimensionless average concentration, absorption rate and absorption efficiency

Fig. 3 shows that the theoretical results for the dimensionless concentration distributions for countercurrent-flow operations in the membrane gas absorption contactor while the average concentration distribution trend tapers along the flow direction in the hollow fiber module and calculated using Eqs. (12) and (13), as indicated from Fig. 4. The theoretical predictions for hollow-fiber module concentration distribution indicated that the concentration changes from the membrane surface to some significant depth into either the water side or gas side, as referred to concentration boundary layers. No significant change in CO_2 concentration occurred on the gas feed side along the transversal coordinate compared to that on the liquid absorbent side because the diffusion coefficient on the gas feed side is much bigger than that on liquid absorbent side. The

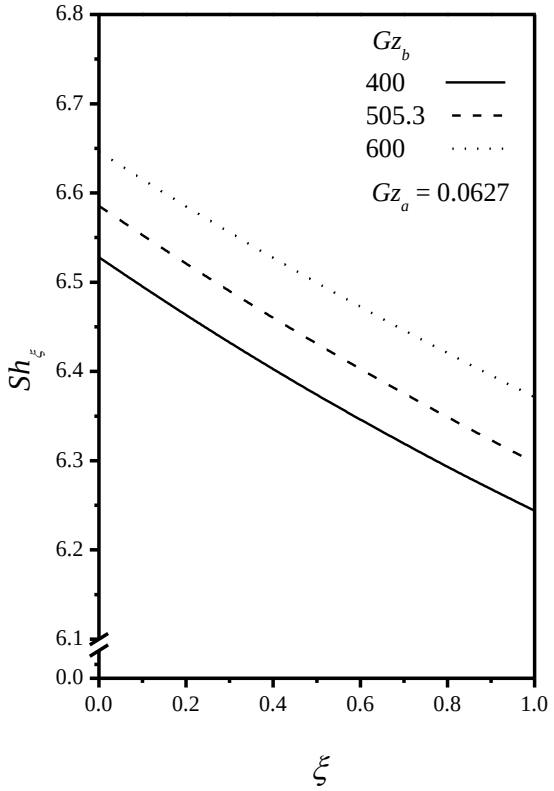

Fig. 5 The local Sherwood number in liquid absorbent within whole membrane contactor with mass-transfer Graetz number Gz_b as a parameter for Gz_a=0.0627

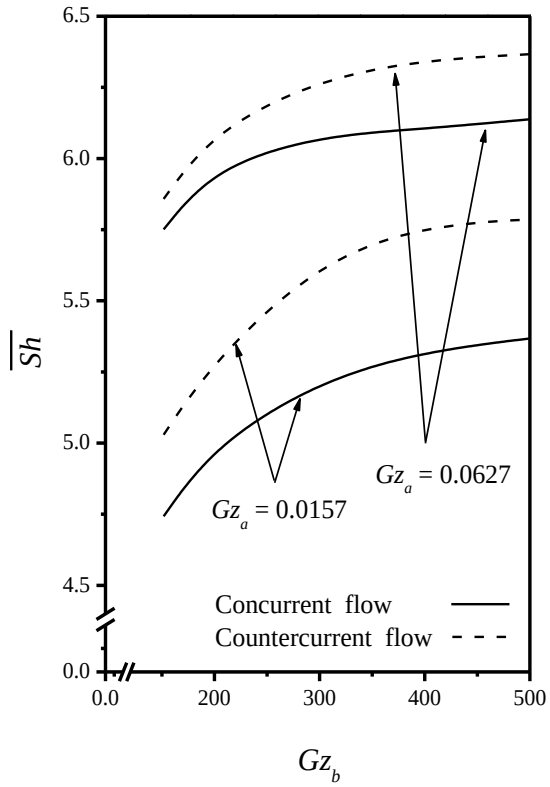

Fig. 6 Average Sherwood number versus mass-transfer Graetz number variations in liquid absorbent with mass-transfer Graetz number in gas feed as a parameter for both flow patterns

average dimensionless concentration distribution in the liquid absorbent $\overline{\psi}_b$ along the fiber length increases with increasing Gz_b, as confirmed from Fig. 4. Each legend for these curves is the transversal concentration distribution calculated using Eqs. (12) and (13) on the specific longitudinal location. The difference in the average concentration distribution increases with increasing Gz_b, and thus, the absorption efficiency is achieved.

Fig. 5 shows the theoretical local Sherwood number $\overline{Sh}$ along the flow direction with mass-transfer Graetz number Gz_b in the liquid absorbent as a parameter and increases with increasing Gz_b when Fig. 6 shows the theoretical average Sherwood numbers $\overline{Sh}$ increase with increasing mass-transfer Graetz numbers Gz_a and Gz_b for both concurrent- and countercurrent-flow operations. As larger mass-transfer Graetz numbers are operated, larger average Sherwood numbers $\overline{Sh}$ are obtained regardless of both concurrent- and countercurrent-flow devices. However, the average Sherwood number in the countercurrent-flow device is larger than that in the concurrent-flow device, as indicated in Fig. 6. Figs. 7 and 8 present graphically the total absorption rate ω and absorption efficiency I_M for both concurrent- and countercurrent-flow operations with inlet CO_2 concentration and mass-transfer Graetz number as parameters, respectively. The theoretical result shows that the total absorption rate ω increases with increasing

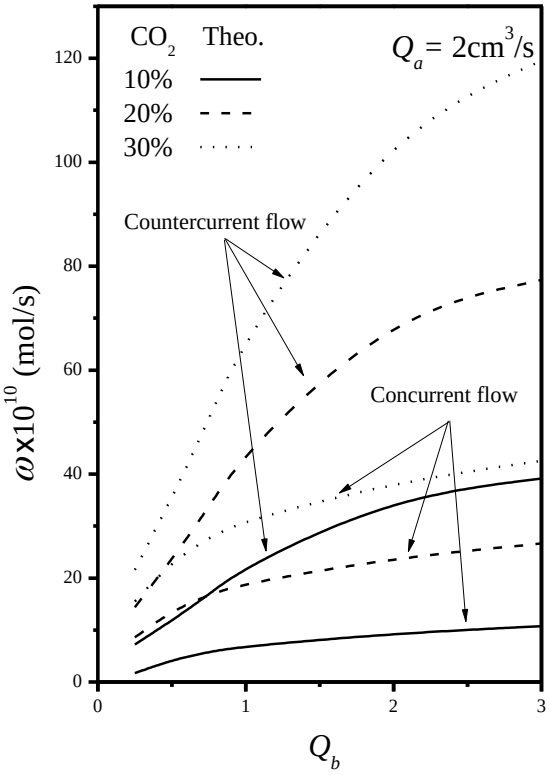

Fig. 7 Comparison of total absorption rate for both flow-type devices (Q_a=2 cm^3/s)

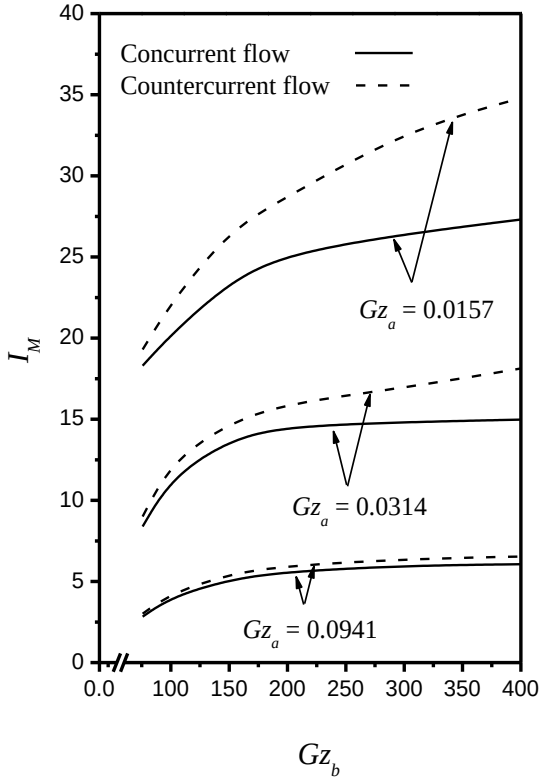

Fig. 8 The absorption efficiency versus mass-transfer Graetz number variations in liquid absorbent with mass-transfer Graetz number in gas feed as a parameter for both flow patterns

the inlet CO_2 concentration in the gas feed stream, as shown in Fig. 7. The increase of the liquid absorbent flow rate Q_b results in the positive effect not only raising the absorption efficiency but also reducing the CO_2 concentration in the liquid outlet stream. The absorption efficiency I_M of gas-liquid membrane absorption were enhanced when Gz_b is increasing or Gz_a is decreasing as well as in the reported gas absorption processes, as indicated in Fig. 8. The absorption efficiency enhancement may be attributed to increasing mass-transfer Graetz number Gz_b associated with the convective mass-transfer coefficient enlargement, resulting in a higher total absorption rate, as confirmed by Fig. 8. Restated, the influence of Gz_b on the gas-liquid membrane absorption is to reduce the concentration boundary layers and create a larger concentration driving force across the membrane surfaces, as shown in Fig. 3. The absorption efficiency enhancement was getting higher rapidly with increasing Gz_b up to the limit of about two hundred, and then leveled off due to the driving-force concentration gradient decreasing under the laminar flow region, especially for operating concurrent-flow devices, however, the total absorption efficiency for both flow-type operations were increasing significantly with increasing Gz_b, as indicated from Fig. 8. The experimental conditions in this study fall in the low Reynolds number region (Re<42) of liquid absorbent side to meet the laminar flow assumption for the mathematical treatments in the present study. The low Reynolds numbers results in lower average Sherwood numbers $\overline{Sh}$ and hence low

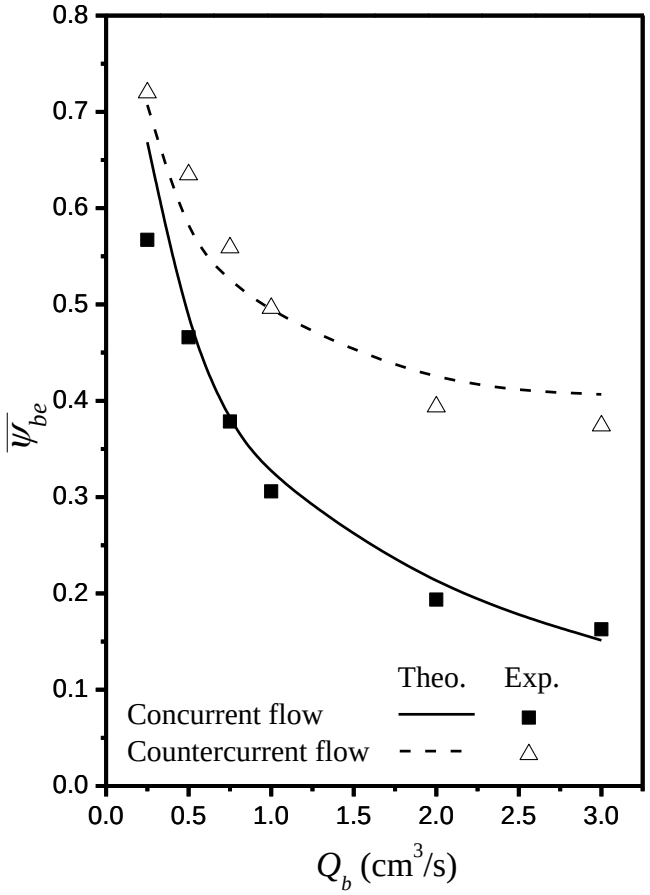

Fig. 9 The average outlet dimensionless concentration versus liquid absorbent flow rate for both concurrent-flow and countercurrent-flow operations

total absorption rate values ω. In practical operations, the Reynolds numbers will be higher and the total absorption rate ω can be enhanced for operating in the turbulent flow region (Kumar, Hogendoorn *et al*. 2002, Wang, Zhang *et al.* 2005, Zhang, Wang *et al.* 2008). It was also found that both the total absorption rate and absorption efficiency in the countercurrent-flow device were larger than those in the concurrent-flow device.

5.2 Experimental analysis

The experimentally and theoretically predicted average outlet dimensionless concentrations for various the liquid absorbent flow rate Q_b in both concurrent-flow and countercurrent-flow configurations are compared in Fig. 9. The average outlet dimensionless concentration significantly decreases with increasing the liquid absorbent flow rate Q_b. The average outlet dimensionless concentration for the countercurrent-flow operation is higher than that for the concurrent-flow operation and the difference is more notable when the liquid absorbent flow rate Q_b is higher. All of these trends are followed by both theoretical and experimental results.

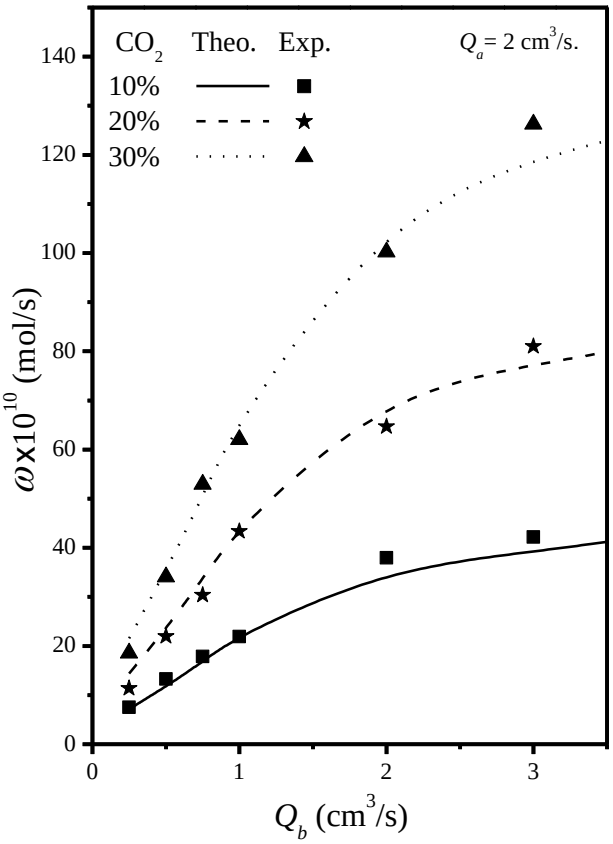

Fig. 10 The total absorption rate of CO_2 versus liquid absorbent flow rate with the initial concentration of CO_2 in gas mixture feed as a parameter for Q_a=2 cm^3/s

Table 3 The accuracy of theoretical predictions

CO_2 concentration (%)	$E = \frac{1}{N}\sum_{i=1}^{N}\frac{\lvert\hat{\omega}_i - \omega_i\rvert}{\hat{\omega}_i}$
10	6.62×10^{-2}
20	8.98×10^{-2}
30	6.94×10^{-2}

Fig. 10 shows the theoretical predictions and experimental data for the total absorption rate versus the liquid absorbent flow rate Q_b for comparisons. The error analysis for the theoretical prediction was validated with the experimental results by defining the accuracy between the theoretical predictions and experimental results as follows

$$E = \frac{1}{N}\sum_{i=1}^{N}\frac{\left|\hat{\omega}_j - \omega_j\right|}{\hat{\omega}_j} \tag{21}$$

where $\hat{\omega}_j$ indicates the theoretical prediction for ω while N and ω_j are the number of experimental measurements and experimental data for ω, respectively. The total absorption rate accuracy was calculated using Eq. (21) for countercurrent-flow operations with $6.62\times10^{-2}\leq E\leq8.98\times10^{-2}$, as shown in Table 3. Both qualitative and quantitative agreements were achieved between the theoretical predictions and experimental results in the hollow fiber gas-liquid membrane contactor under countercurrent-flow operations.

6. Conclusions

The laminar countercurrent-flow hollow-fiber membrane gas absorption module mass transfer efficiency was investigated theoretically and experimentally. A two-dimensional mass-transfer mathematical formulation was solved analytically using Happel's free surface model to develop the velocity profile, and thus, the solutions for such conjugated Graetz problems were performed using the orthogonal technique in expanding the eigenfunction of an extended power series. The advantages and values of the present two-dimensional mathematical model are that the concentration distribution, total absorption rate and average Sherwood number in the hollow fiber module can be calculated directly from the simplified expressions without requiring experimental data interpolation. Therefore, those useful graphical presentations make us better understand how important operating condition selection is in achieving higher performance in hollow fiber gas-liquid membrane contactors. This is the value of the present work. The liquid absorbent flow rate, gas feed flow rate and initial CO_2 concentrations influences on the gas feed on both total absorption rate and absorption efficiency were discussed in this study. The results show that the gas feed flow rate had a significant influence on the mass transfer behavior in the membrane gas absorption operations, especially for countercurrent-flow devices, as indicated in Figs. 7 and 8. It was also seen from the theoretical predictions and experimental runs that the total absorption rate increases with increasing mass-transfer Graetz number in the liquid absorbent.

The enhancement of both absorption efficiency and total absorption rate may be attributed to increasing the liquid absorbent flow rate and thus strengthening the convective mass-transfer coefficient. Restated, the reduction in concentration polarization with increasing fluid flow rates is accomplished in thinning both the velocity boundary and concentration boundary layers, resulting in a larger driving-force concentration gradient, and hence, establishing a higher trans-membrane mass transfer across the membrane surfaces, as inferred from Figs. 8 and 10, respectively. The accuracy of the theoretical predictions was estimated to be $6.62\times10^{-2}\leq E\leq8.98\times10^{-2}$ for countercurrent-flow devices. The theoretical results show that the present model can well simulate the mass transfer behavior of a hollow fiber gas-liquid membrane contactor with performing the validation using the experimental data. One can also expect that the present mathematical treatment can be applied to other hollow fiber modules in membrane separation processes coupled with both heat- and mass-transfer problems, which have not previously been solved in detail.

Acknowledgements

The authors wish to thank the Ministry of Science and Technology of the Republic of China for the financial support.

References

Al-Marzouqi, M.E., El-Nass, M.H., Mzrzouk, S.A.M., Al-Zarooni, M.A., Abdullatif, N. and Faiz, R. (2008), "Modeling of CO_2 absorption in membrane contactors", *Sep. Purif. Technol.*, **59**, 286-293.

Bothuna, G.D., Knutsona, B.L., Strobelb, H.J., Nokesc, S.E., Brignoled, E.A. and Díazd, S. (2003), "Compressed solvents for the extraction of fermentation products within a hollow fiber membrane contactor", *J. sSpercrit. Fluid.*, **25**, 119-134.

Costello, M.J., Fane, A.G., Hogan, P.A. and Schofield, R.W. (1993), "The effect of shell side hydrodynamics on the performance of axial flow hollow fiber modules", *J. Membr. Sci*., **80**, 1-11.

Davis, E.J. and Venkatesh S. (1979), "The solution of conjugated multiphase heat and mass transfer problems, *Chem. Eng. J*., **34**, 775-787.

Dindore, V.Y., Brilman, D.W.F., Feron, P.H.M. and Versteeg G.F. (2004), "CO_2 absorption at elevated pressures using a hollow fiber membrane contactor", *J. Membr. Sci*., **235**, 99-109.

Gabelman, A. and Hwang, S.T. (1999), "Hollow Fiber Membrane Contactors", *J. Membr. Sci.*, **159,** 61-106.

Happel, J. (1959), "Viscous flow relative to arrays of cylinder", *AIChE J*., **5**, 174-177.

Ho, C.D., Sung, Y.J. and Chuang, Y.C. (2013), "An analytical study of laminar concurrent flow membrane absorption through a hollow fiber gas-liquid membrane contactor", *J. Membr. Sci*., **428**, 232-240.

Ho, C.D., Yeh, H.M. and Sheu W.S. (1998), "An analytical study of heat and mass transfer through a parallel-plate channel with recycle", *Int. J. Heat Mass Transfer*, **41**, 2589-2599.

Karoor, S. and Sirkar, K.K. (1993), "Gas absorption studies in microporous hollow fiber membrane modules", *Ind. Eng. Chem. Res*., **32**, 674-684.

Kim, Y.S. and Yang, S.M. (2000), "Absorption of carbon dioxide through hollow fiber membranes using various aqueous absorbents", *Sep. Purif. Technol*., **21**, 101-109.

Kumar, P.S., Hogendoorn, J.A., Ferron, P.H.M. and Versteeg, G.F. (2002), "New absorption liquids for the removal of CO_2 from dilute gas streams using membrane contactos", *Chem. Eng. Sci.*, **57**, 1639-51.

Laouinia, A., Jaafar-Maaleja, C., Sfarb, S., Charcosseta, C. and Fessia, H. (2011), "Liposome preparation using a hollow fiber membrane contactor - Application to spironolactone encapsulation", *Int. J. Pharm.*, **415**, 53-61.

Lee, Y., Noble, R.D., Yeom, B.Y., Park, Y.I. and Lee, K.H. (2001), "Analysis of CO_2 removal by hollow fiber membrane contactors", *J. Membr. Sci*., **194**, 57-67.

Li, K. and Teo, W.K. (1998), "Use of permeation and absorption methods for CO_2 removal in hollow fiber membrane modules", *Sep. Purif. Technol*., **13**, 79-88.

Li, R., Xu, J., Wang, L., Li, J. and Sun X. (2009), "Reduction of VOC emissions by a membrane-based gas absorption process", *J. Envirn. Sci.*, **21**, 1096-1102.

Mavroudi, M., Kaldis, S.P. and Sakellaropoulos, G.P. (2003), "Reduction of CO_2 emissions by a membrane contacting process", *Fuel.*, **82**, 2153-2159.

Nunge, R.J. and Gill, W.N. (1966), "An analytical study of laminar counterflow double-pipe heat exchangers", *AIChE J.*, **12**, 279-289.

Papoutsakis, E. and Ramkrishna D. (1981), "Conjugated Graetz problems. i: general formalism and a class of solid-fluid problems", *Chem. Eng. Sci.*, **36**, 1381-1390.

Perelman, T.L. (1961), "On conjugated problems of heat transfer", *Int. J. Heat Mass Transfer*, **3**, 293-303.

Qi, Z. and Cussler E.L. (1985a), "Microporous hollow fibers for gas absorption: I. Mass transfer in the liquid", *J. Membr. Sci.*, **23**, 321-332.

Qi, Z. and Cussler E.L. (1985b), "Microporous hollow fibers for gas absorption: II. Mass transfer across the membrane", *J. Membr. Sci.*, **23**, 333-345.

Ramakula, P., Prapasawada, T., Pancharoena, U. and Pattaveekongkab, W. (2007), "Separation of radioactive metal ions by hollow fiber-supported liquid membrane and permeability analysis", *J. Chin. Inst. Chem. Eng.*, **38**, 489-494.

Rezakazemi, M., Shirazian, S. and Ashrafizadeh S.N. (2012), "Simulation of ammonia removal from industrial wastewater streams by means of a hollow-fiber membrane contactor", *Desalination*, **285**,

383-392.
Varavuth, S., Jiraratananon, R. and Atchariyawut S. (2009), "Experimental study on dealcoholization of wine by osmotic distillation process", *Sep. Purif. Technol*., **66**, 313-321.
Versteeg, G.F. and van Swaaij, W.P.M. (1988), "Solubility and diffusivity of acid gases (CO_2, N_2O) in aqueous alkanolamine solutions", *J. Chem. Eng. Data*, **33**, 29-34.
Wang, R., Zhang, H.Y., Feron, P.H.M. and Liang, D.T. (2005), "Influence of membrane wetting on CO_2 capture in microporous hollow fiber membrane contactors", *Sep. Purif. Technol.*, **46**, 33-40.
Wang, W.P., Lin, H.T. and Ho, C.D. (2006), "An analytical study of laminar co-current flow gas absorption through a parallel-plate gas-liquid membrane contactor", *J. Membr. Sci.*, **278**, 181-189.
Yang, M.C. and Cussler E.L. (1986), "Designing hollow-fiber contactor", *AIChE J*., **32**, 1910-1915.
Zhang, H.Y., Wang, R., Liang, D.T. and Tay, J.H. (2008), "Theoretical and experimental studies of membrane wetting in the membrane gas-liquid contacting process for CO_2 absorption", *J. Membr. Sci.*, **194**, 162-170.
Zheng, J.M., Xu, Y.Y. and Xu, Z.K. (2003), "Shell side mass transfer characteristics in a parallel flow hollow fiber membrane modules", *Sep. Sci. Tech*., **6**, 1247-1267.

ED

Nomenclature

C concentration in the stream (mol/m^3)
D_{AB} ordinary diffusion coefficient of CO_2 in N_2 (m^2/s)
D_{AC} ordinary diffusion coefficient of CO_2 in water (m^2/s)
D_{eq} the equivalent diameter of channel b (m)
E the accuracy of the experimental results
F_m eigenfunction associated with eigenvalue λ_m
G_m function defined during the use of orthogonal expansion method
Gz mass-transfer Graetz number
H Henry's law constant
I_M absorption efficiency
$k_{b\xi}$ local mass transfer coefficient for liquid phase
L channel length (m)
N the number of experimental measurements
Q input volumetric flow rate (m^3/s)
r transversal coordinate (m)
r_f free surface radius (m)
r_i fiber inside radius (m)
r_o fiber outside radius (m)
r_s shell outside radius (m)
S_m expansion coefficient associated with eigenvalue λ_m
Sh_ξ local Sherwood number
$\overline{Sh}$ average Sherwood number
v velocity distribution of fluid (m/s)
$\bar{v}$ average velocity of fluid (m/s)
z longitudinal coordinate (m)

Greek letters

δ thickness of the porous membrane (m)
ε membrane permeability
ϕ packing density
η dimensionless transversal coordinate, r/r_f
λ_m eigenvalue
ξ dimensionless longitudinal coordinate, z/L
ψ dimensionless concentration
$\overline{\psi}$ average dimensionless concentration
ω absorption rate (mol/s)
ω_j experimental data of ω
$\hat{\omega}_j$ theoretical prediction of ω

Superscripts and subscripts

a in the gas feed flow channel
b in the liquid absorbent flow channel
i at the inlet
e at the outlet